Available online at www.sciencedirect.com
ScienceDirect
Applied Catalysis B: Environmental 80 (2008) 156–167
APPLIED CATALYSIS B: ENVIRONMENTAL
www.elsevier.com/locate/apcatb

# Transmission electron microscopic observation on reduction process of copper–iron spinel catalyst for steam reforming of dimethyl ether

K. Eguchi [a,*], N. Shimoda [a], K. Faungnawakij [a,b], T. Matsui [a], R. Kikuchi [a], S. Kawashima [b]

[a] Department of Energy and Hydrocarbon Chemistry, Graduate School of Engineering, Kyoto University, Nishikyo-ku, Kyoto 615-8510, Japan
[b] Japan Science and Technology Agency (JST), JST Innovation Plaza Kyoto, Goryo-Ohara Nishikyo-ku, Kyoto 615-8245, Japan

Received 27 July 2006; received in revised form 24 October 2007; accepted 16 November 2007
Available online 10 January 2008

**Abstract**

The reduction process of copper–iron spinel oxide, which is active for steam reforming of dimethyl ether after mixing with alumina, has been investigated by a transmission electron microscope (TEM), scanning TEM (STEM), and energy dispersive X-ray (EDX) analyzer. The catalyst preparation was started from formation of well-sintered $CuFe_2O_4$ by calcination in air at 900 °C. After reduction of $CuFe_2O_4$ with hydrogen at 250 °C, metallic copper grains were developed on reduced spinel surface by the phase separation from the oxide. Strong chemical interaction between deposited Cu and reduced spinel oxide was expected from their intimate interfacial contact and lattice matching. The reduced sample contained metallic Cu, reduced spinel, and spinel oxide with super-lattice structure. Partial elimination of Cu and lattice oxygen resulted in formation of pores in and between the oxide grains. The size of the deposited Cu particle and Cu grain was largely distributed. After heating at higher temperature of 350 °C, the large spinel oxide particles are decomposed into small particles via formation of cracks. The resultant catalyst powder was very porous and consisted of very small particles of Cu, iron oxide, and spinel oxide. STEM–EDX analyses clarified the phase separation process of metallic Cu and iron oxide from host $CuFe_2O_4$ upon reduction.


*Keywords:* TEM; EDX; $CuFe_2O_4$ spinel; Reduction; Dimethyl ether; Steam reforming

## 1. Introduction

Polymer electrolyte fuel cells (PEFCs) have been regarded as clean and highly efficient power generators for stationary and mobile use [1–3]. Recently, dimethyl ether (DME) has attracted much attention as a $H_2$ source as well as an alternative fuel for diesel engine with clean exhaust. Catalytic hydrogen production from dimethyl ether has been proposed by Amoco Corp. in 1996 as hydroshift reaction [4]. Dimethyl ether can be reformed at lower temperatures than hydrocarbons [5,6]. Dimethyl ether shows a good potential to be used as a $H_2$ source for automotive PEFC system [7], since this fuel molecule can be reformed at lower temperatures than hydrocarbons [8–17]. As DME molecules possess no C–C bond, carbon deposition can be avoided easily by adding water in the reaction system. It was suggested that sufficiently low cost should be achieved by producing in a large scale, though the cost problem is still controversial. As for the safety to toxicity, DME is preferable to methanol [10,12]. Production of hydrogen from DME can be achieved through catalytic reactions, such as steam reforming, partial oxidation, and autothermal reforming [17–19].

Steam reforming of DME can be expressed as a combination of hydrolysis of DME (reaction (1)) and steam reforming (SR) of methanol (reaction (2)):

$$(CH_3)_2O + H_2O \rightarrow 2CH_3OH \quad (1)$$

$$CH_3OH + H_2O \rightarrow CO_2 + 3H_2 \quad (2)$$

From reactions (1) and (2), overall DME steam reforming can be expressed as follows:

$$(CH_3)_2O + 3H_2O \rightarrow 2CO_2 + 6H_2 \quad (3)$$

Copper-based catalysts have been known to be active for reforming of methanol (step (2)), while solid-acid catalysts

* Corresponding author. Tel.: +81 75 383 2519; fax: +81 75 383 2520.
*E-mail address:* eguchi@scl.kyoto-u.ac.jp (K. Eguchi).

0926-3373/$ – see front matter © 2007 Elsevier B.V. All rights reserved.
doi:10.1016/j.apcatb.2007.11.020

are commonly used for hydrolysis of DME (step (1)) [8–17]. We have proposed copper-based spinel catalysts for a series of reactions; i.e., water gas shift reaction (WGSR) and steam reforming of methanol and DME [13,17,20,21]. For the application to steam reforming of DME copper–iron spinel mixed with γ-alumina was the most active in the temperature range of 350–450 °C among the spinel oxide-based catalysts investigated. The activity was found to be higher than the commercial $Cu/ZnO/Al_2O_3$ catalysts when the $CuFe_2O_4$ catalyst was mixed with γ-alumina [22]. In this temperature range, on weakly acidic sites of γ-alumina, the reaction (1) proceeds without significant formation of decomposition products such as methane or carbonaceous compounds [13]. Zeolite or acidic catalysts were more active for this step, but the strong acidity gave rise to unselective decomposition to methane and carbonaceous species at the temperature desirable for the second step [22]. The second reaction is conducted on Cu which is deposited by phase separation from the spinel oxide in the proposed catalyst. This Cu-spinel catalyst attained the sufficient activity for complete conversion of methanol in the temperature range of 350–450 °C. For the DME reforming at lower temperatures, Cu catalysts do not exhibit enough activities, whereas at higher temperature range unselective decomposition and sintering of Cu led to deactivation of catalysts [17,22].

The activation of the Cu-based spinel catalyst is indispensable for the use in WGSR and DME reforming; i.e., the pretreatment composed of calcination in air at around 900 °C and subsequent reduction with $H_2$ or in reaction gases at around 250–350 °C [17,21]. The initial calcination in air is for the complete formation of spinel phase, and the following reduction treatment for the deposition into active $Cu^0$ species and pore formation. The oxidation state of copper in spinel is divalent, whereas reduction to metallic state was observed for spent catalysts by X-ray diffraction. This suggests that the reduction process as well as reduced state of copper in the spinel catalyst is important in elucidating the catalytic properties of the copper-based spinel catalysts. The present investigation focused on the structural analysis of $CuFe_2O_4$ spinel that demonstrated high activity for DME reforming after mixing with γ-alumina. Reduction process of the spinel oxide and subsequent deposition of active copper species were observed by high resolution transmission electron microscope (HR-TEM). A composition and dispersion on nm scale was analyzed by scanning TEM (STEM) with energy dispersive X-ray (EDX) analysis.

## 2. Experimental

### 2.1. Catalyst preparation

The spinel-type oxide catalyst, $CuFe_2O_4$, was prepared from corresponding nitrate mixture and subsequent solid state reaction with the citrate process. The atomic ratio of Cu to Fe was fixed at 1:2 which is stoichiometric for the formation of spinel-type oxide. An aqueous solution of $Cu(NO_3)_2$ and $Fe(NO_3)_3$ (Nacalai Tesque, Analytical Grade) was stirred at 60 °C for 1 h and heated to 90 °C to evaporate $H_2O$. The precipitate was heated to 140–200 °C to decompose citric acid until fine oxide powders were obtained. The obtained powders were calcined in air at 900 °C for 10 h for Cu-based spinel-oxide type catalysts. The heat treatment at high temperature and complete formation of spinel phase was indispensable in deriving high activity for water gas shift reaction [21] as well as DME reforming [17]. Reduction treatment of catalyst was carried out at 250 °C or 350 °C for 1 h in 10% $H_2/N_2$ in a flow system.

The catalytic reforming of DME is carried out at 350 °C and a little higher temperature over $CuFe_2O_4$ + γ-$Al_2O_3$ and $Cu/ZnO/Al_2O_3$ catalysts, respectively [13]. Thus, the catalyst after reduction treatment at 350 °C may reflect the working state. The effect of reduction treatment on the catalytic activity will be explained in Section 3. The catalyst for steam reforming of DME was prepared by mechanical mixing of spinel oxide, $CuFe_2O_4$, with γ-alumina (ALO-8, Catalysis Soc., Japan), since the spinel-based catalyst does not possess acidic center for hydrolysis (reaction (1)). The Cu spinel was physically mixed with the γ-alumina catalyst at a fixed weight ratio of 2:1 [22]. However, the present TEM observation was focused on the phase transformation and microstructural change of the spinel oxide in a reduced state. Therefore, the observation was made only for reduced $CuFe_2O_4$ samples without alumina.

### 2.2. Catalytic performance measurement

Catalytic activities for steam reforming of DME were evaluated under atmospheric pressure in a packed bed reactor. Prior to the evaluation, reduction of the catalyst composed of the mixture of $CuFe_2O_4$ and γ-alumina was carried out at 250 °C and 350 °C in the following manner [22]. A catalyst was heated in the $N_2$ flow; then the reduction was performed in 10% $H_2/N_2$ at 250 °C or 350 °C for 0.5 h. The reduced catalyst was then set at the reaction temperature in $N_2$ flow prior to the reaction tests. A mixture of steam, DME, and $N_2$ at a desired steam-to-carbon ratio (S/C) was supplied through mass flow controllers to a pre-heater at temperature of 150 °C, and then to the catalyst bed at 350 °C. For the time-on stream measurement, the gas analysis was periodically carried out. Compositions of influent and effluent gas were analyzed by on-line gas chromatographs equipped with FID (Shimadzu, GC-9A) and TCD (VARIAN, CP-4900). The steam in the feed and reformate was trapped by a condenser before the gas analysis. A Poraplot U column was used for separation of DME, MeOH, and $CO_2$, and a molecular sieve 5A column was used for separation of $H_2$, $N_2$, $CH_4$, and CO.

### 2.3. TEM observation

The spinel catalyst powder thus obtained was embedded in a resin. The bulky resin sample containing the catalyst powder was sliced and thin flaky sample was mechanically ground. The thin specimen preparation was followed by ion milling with GATAN, Dual Mill 600. The samples were mounted on Mo grid for the TEM, STEM–EDX observation.

Transmission electron microscope (TEM, Hitachi H-9000UHR III) with an acceleration voltage of 300 kV was used for observation of microstructure, high resolution TEM image, and diffraction image.

Scanning TEM–energy dispersive X-ray (STEM–EDX) analysis was performed by HR-TEM (JEOL, JEM2100F) equipped with field emission electron source with an accelerating voltage of 200 kV equipped with a JEOL JED-2300T detector (energy resolution < 133 eV). Secondary X-ray from the sample was analyzed with an energy dispersive X-ray spectrometer with a Si–Li solid state detector and an ultra-thin window. Measurement was carried out with a focused electron beam of 1 nm in diameter. The acquisition time for EDX was generally 30 s for point X-ray analysis, and 40 min for X-ray imaging. An annular detector installed on the STEM system has been utilized for imaging with elastically scattered electrons. The high angle annular dark field (HAADF) image of the multi-phase sample is effective in distinguishing the domains with different atomic number. The HAADF image was, therefore, taken to reference to the X-ray images of oxygen, iron, and copper to clarify the local compositional distribution. The image was obtained by an analysis station and Gatan DigiScan II.

## 3. Results and discussion

### 3.1. Catalytic activity of spinal alumina catalyst for dimethyl ether reforming

Steam reforming of DME proceeds by the two-step catalytic reaction as mentioned above. After examination of various acidic catalysts for hydrolysis of DME to methanol (reaction (1)) and copper-based catalysts for steam reforming of methanol (reaction (2)), we selected the catalyst composed of $CuFe_2O_4$ and γ-alumina [13,22]. The reaction was carried out at 350 °C to clarify the difference in catalytic activities of the catalysts. The mechanical mixture of γ-alumina and copper–iron spinel ($CuFe_2O_4$) was found to be active for this reaction. Fig. 1 shows the time course of the catalytic activity of $CuFe_2O_4$ + γ-alumina catalyst after pre-reduction treatment with $H_2$. The activity for the $CuFe_2O_4$ was negligibly small; indicating that γ-alumina is indispensable for the first step of reaction (1). The catalytic activity for after reduction with hydrogen indicated that the catalysts reduced at different temperatures displayed almost the same level of activity after 1 h from the start of the reaction. The steady state activity level was almost the same as that of the $CuFe_2O_4$ + γ-alumina catalyst without reduction [22], but the induction period required for the catalyst to reach to the steady state was shorter for the sample with the reduction treatment. Especially, the reduction at 350 °C was effective to attain steady state shortly. Cu-species accommodated in the spinel phase was reduced to the active metallic copper species. Thus, the reduction treatment corresponds to the activation process of the catalyst. The steady state activity was easily attained for the catalyst prereduced at 350 °C than at 250 °C. Thus, it is considered that the activation process and morphological change after

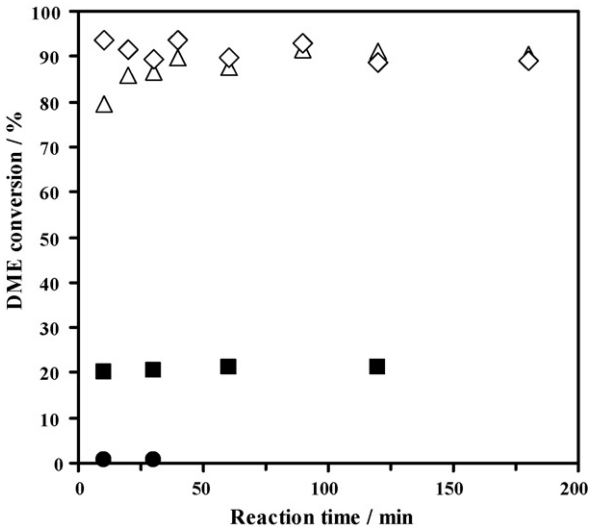


Fig. 1. DME conversion vs. reaction time in DME SR over $CuFe_2O_4$ + $Al_2O_3$ reduced at 350 °C (◇), $CuFe_2O_4$ + $Al_2O_3$ reduced at 250 °C (△), Cu/ZnO/$Al_2O_3$ + $Al_2O_3$ reduced at 250 °C (■), and $CuFe_2O_4$ reduced at 250 °C (●). Reduction condition: 10% $H_2/N_2$ for 3 h. Reaction condition: 350 °C; S/C = 2.5; GHSV = 2000 $h^{-1}$.

reduction at 250 °C and 350 °C were observed by TEM. The activity of commercially available Cu/ZnO/$Al_2O_3$ was also listed in the figure, but was lower than the $CuFe_2O_4$ + γ-alumina catalyst.

The morphology of calcined $CuFe_2O_4$ observed by SEM before reduction or reaction is shown in Fig. 2. Well-sintered microstructure was obvious after calcination in air at 900 °C. The TEM photograph of this unreduced sample consisted only of uniform contrast and did not indicate any open or closed pores. This TEM image was not presented herein, since no textural information was observed. The surface area and pore volume measured by nitrogen adsorption is summarized in Table 1. As the unreduced $CuFe_2O_4$ + γ-alumina was calcined

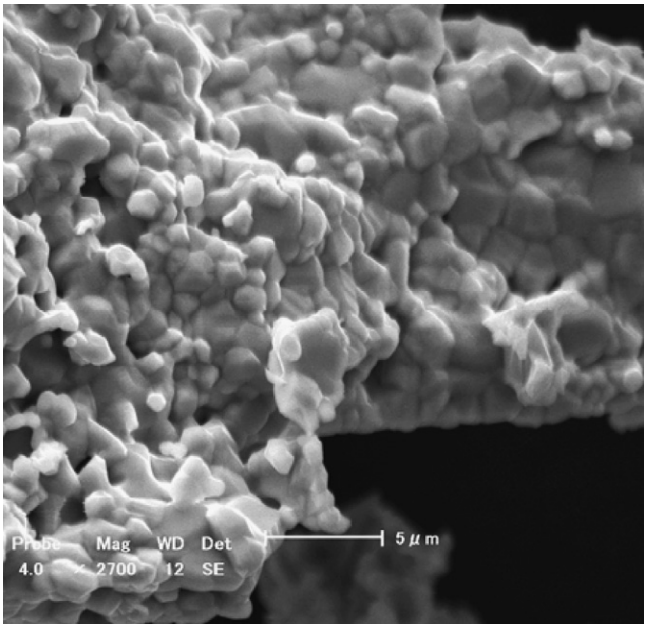


Fig. 2. SEM image of $CuFe_2O_4$ calcined at 900 °C before reduction process.

Table 1
Porosity and BET surface area of $CuFe_2O_4$ before and after reduction process

| Catalyst | BET surface area ($m^2\ g^{-1}$) | Pore volume ($\times 10^{-3}\ cm^3\ g^{-1}$) |
|---|---|---|
| $CuFe_2O_4$ unreduced | 0.3 | 0.89 |
| $CuFe_2O_4$ reduced at 250 °C | 0.6 | 3.33 |
| $CuFe_2O_4$ reduced at 350 °C | 3.4 | 13.91 |

Reduction condition: 10% $H_2/N_2$ for 3 h.

at 900 °C for complete spinel formation, the surface area and pore volume were extremely small to be used as catalysts. The surface area and pore volume of $CuFe_2O_4$ spinel was increased upon reduction with $H_2$, and especially when the reduction temperature was raised to 350 °C. This increase corresponds to the phase change into metallic Cu and reduced iron oxide during the course of the reduction. Evaluation of the surface area of metallic Cu may support the analysis of intrinsic activity of respective species. However, evaluation by adsorption technique such as $N_2O$ adsorption was not applicable to the reduced $CuFe_2O_4$ because of the adsorption of $N_2O$ on reduced spinel and iron oxides.

We have reported previously on the catalytic activities of spinel oxides and transition metal oxides for methanol reforming [13]. The catalytic activity of Fe oxide catalyst for steam reforming of methanol was significantly lower than that of $Cu/ZnO/Al_2O_3$ or $CuFe_2O_4$ (only 5% conversion at 350 °C). Thus, the Cu species in the spinel is attributed to the

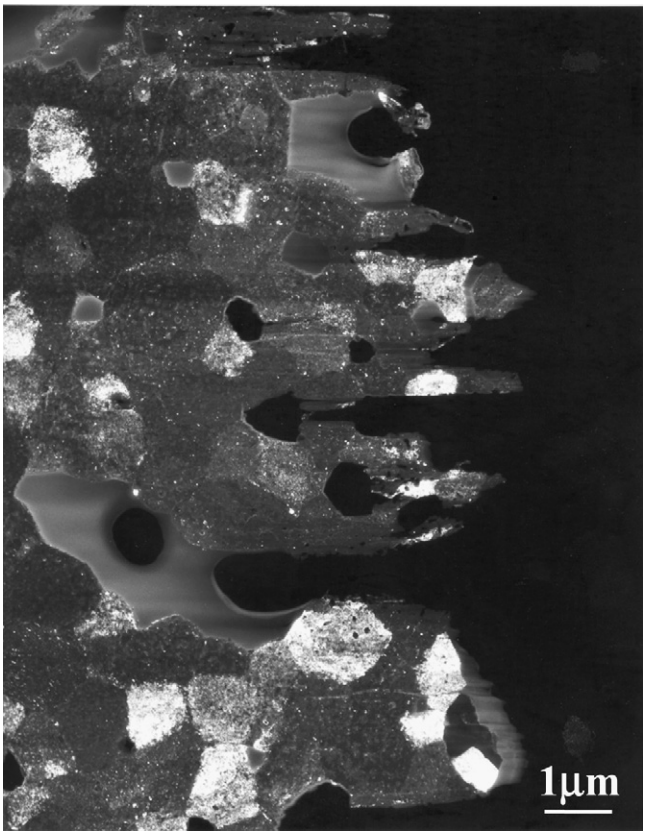


Fig. 4. Dark field image obtained from diffraction of Cu in $CuFe_2O_4$ reduced at 250 °C.

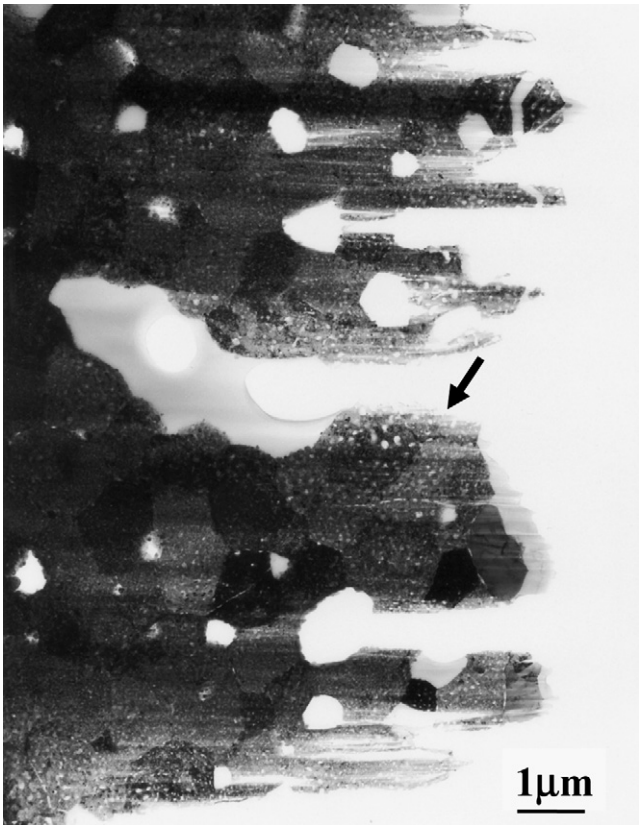


Fig. 3. Bright field TEM image of $CuFe_2O_4$ reduced with $H_2$ at 250 °C. The arrow in the figure indicates an example of a single crystalline spinel grain.

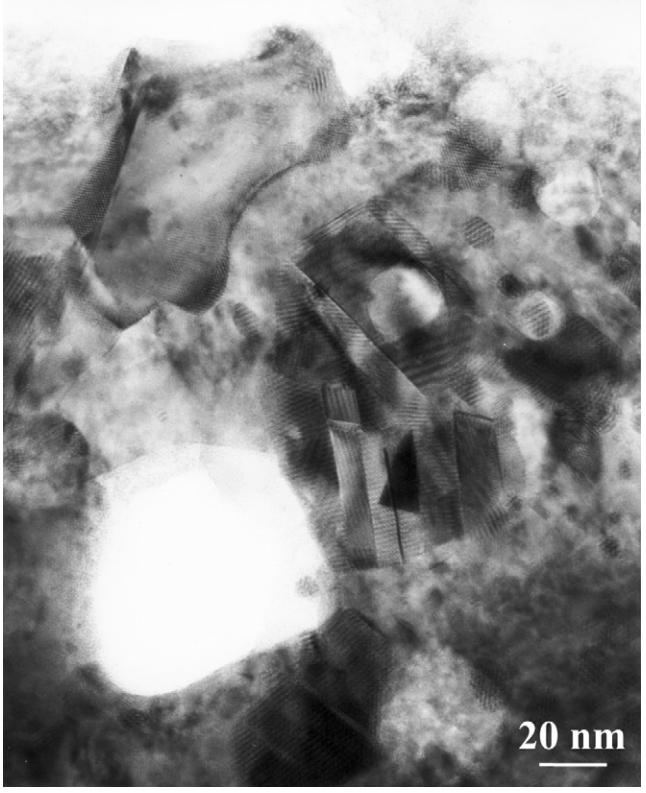


Fig. 5. HR-TEM image of $CuFe_2O_4$ reduced at 250 °C.

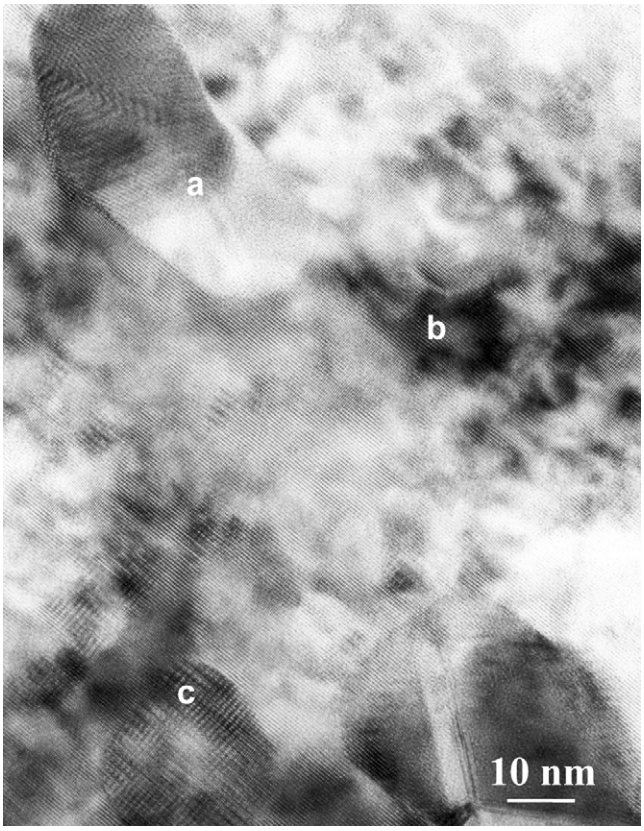


Fig. 6. HR-TEM image of $CuFe_2O_4$ reduced at 250 °C for selected area diffraction (SAD) patterns in Fig. 7.

active center for methanol reforming. The X-ray diffraction pattern of the $CuFe_2O_4$ catalyst after reduction or after steam reforming of methanol or DME showed only diffraction lines from Cu metal and $Fe_3O_4$, thus the formation process of Cu metal in the spinel catalyst should be important in determining the catalytic activity for the series of reaction [17].

### 3.2. High resolution TEM observation of $CuFe_2O_4$ spinel oxide reduced at 250 °C

Metallic copper particles have been known to be active for reaction step (2) in steam reforming of DME [9,13,17]. Generally, Cu catalysts were prepared by impregnating Cu solution into alumina support or by coprecipitation process.

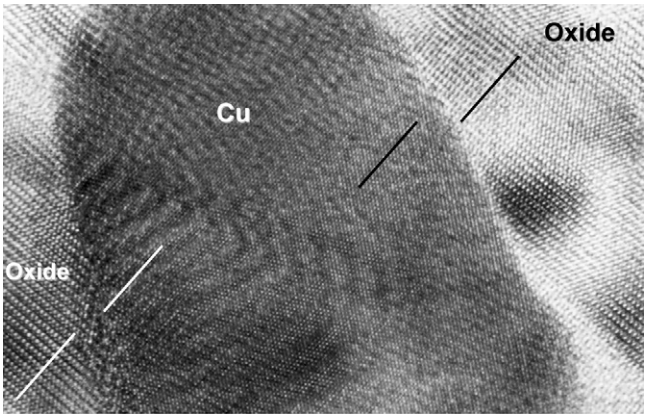


Fig. 8. High resolution image for region a in Fig. 6.

The current preparation procedure started from the preparation of a homogeneous oxide phase of spinel. The phase separation and grain growth process on reduction is, therefore, important for this catalyst system. The formation process and the structure of the reduced spinel catalyst were observed by high resolution transmission microscope. Cu and Fe ions occupy respective cationic sites in the spinel structure of $CuFe_2O_4$. Upon exposure of $CuFe_2O_4$ spinel oxide to hydrogen at 250 °C, copper and iron components are reduced to metallic copper and reduced iron oxide; the valence reduction inevitably accompanies phase separation of oxide and metal phases. Copper ions can be easily reduced to the metallic state, and then the reduced fine particles aggregate to form fine deposits.

A bright field image of the catalyst reduced with hydrogen at 250 °C is shown in Fig. 3. The whole region was continuous and consisted of a large particle, whereas the grains with different contrasts contacted tightly with each other. Large continuous regions in TEM photographs are hereafter called as particles and the domains with different contrasts in a particle are called as grains. The large particles should reflect well-sintered spinel oxide and the grains in such large particles were formed due to phase separation with reduction at 250 °C. This microstructure implies that each grain was basically formed upon reduction in the sintered polycrystal of the original spinel, but the obvious difference in contrast among grains indicates the state of a multi-phasic composite. The grains with their size of 0.5–1 μm are ascribed to oxide and deposited copper phases which were

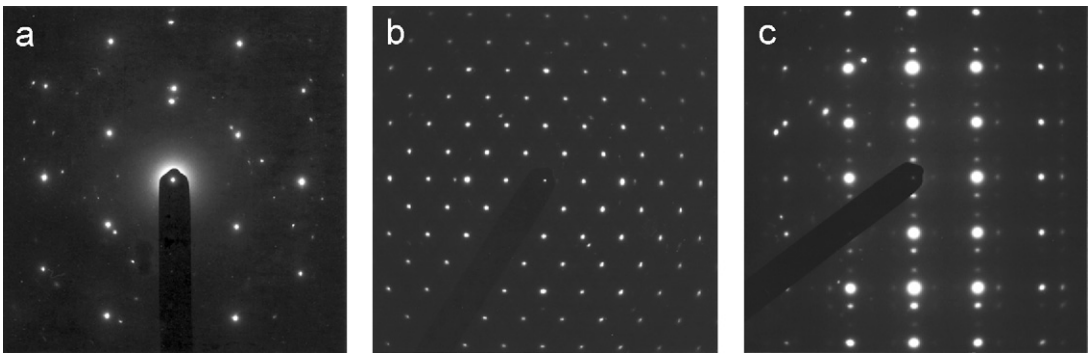


Fig. 7. Selected area diffraction (SAD) patterns of $CuFe_2O_4$ reduced at 250 °C. SAD patterns were obtained from the designated positions (a–c) in Fig. 6.

formed from the single spinel phase with reduction. A number of voids with their size ranging from 0.1 to 1 μm were formed in some grains. It is noted that even in the single grain (indicated by an arrow) a number of bright spots have been observed with their size of 10–50 nm. Though each grain was single crystalline judging from the absence of grain boundary, the contrast in the grain was not homogeneous. Some grains contained number of bright spots of *ca*. 10 nm in size. These spots are expected to correspond to heterogeneity in thickness of the oxide. The reduction of spinel oxide and subsequent exclusion of metallic copper proceeded inhomogeneously. Thus, the surface of the reduced oxide was roughened because of the pores and dimples formed via partial elimination of Cu and O species. Metallic copper could be observable as separated particles whose sizes were largely distributed.

A dark field image of the same region has been observed by using ⟨1 1 1⟩ diffraction of metallic Cu as shown in Fig. 4. In this image every particle and grain with a bright contrast could be attributed to metallic copper species. Some large Cu particles of 0.5–1 μm in diameter have been grown as a result of the phase separation from the spinel oxide and the subsequent coarsening by sintering. Although the region with darker contrast image corresponded to original or reduced spinel grains, which can be clearly distinguished from the bright Cu grains. Cracks or voids were not observed at the contacting interfaces between the spinel grains or between Cu and spinel grains with different contrasts; i.e., rather intimate contact at the grain boundaries was generally observable for reduced oxide and metal grains. This implies strong adhesion and chemical interaction between original oxide and deposited Cu even after phase separation of them. In addition to the large Cu particles, fine particles with bright image were dispersed on the dark images of spinel or reduced oxide phases. The particle size of finely deposited Cu was less than 50 nm and was not uniform. It is considered that fine particles of Cu are responsible for high activity for reforming of methanol as reaction step (2).

A high resolution TEM image was observed for analysis of the separated phases from lattice images. As can be judged from lattice image in Fig. 5, the sample consisted of only crystalline grains without amorphous region. This agglomerated particle involved a large void in the central part with its diameter of 50 nm. The peripheral area consisted of large crystalline grains in addition to a number of overlapping small grains with different orientations.

From the high resolution image of Fig. 6, the phases comprised in the sample reduced at 250 °C were attributed by also taking the selected area diffraction (SAD) pattern of typical regions, as shown in Fig. 7. The particle image with its diameter of 30–40 nm marked by the region a in Fig. 6 was metallic copper judging from its lattice spacing. The diffraction pattern in Fig. 7a agreed with the reported lattice constant of metallic copper (JCPDS: 04-0836). The pattern in Fig. 7b was

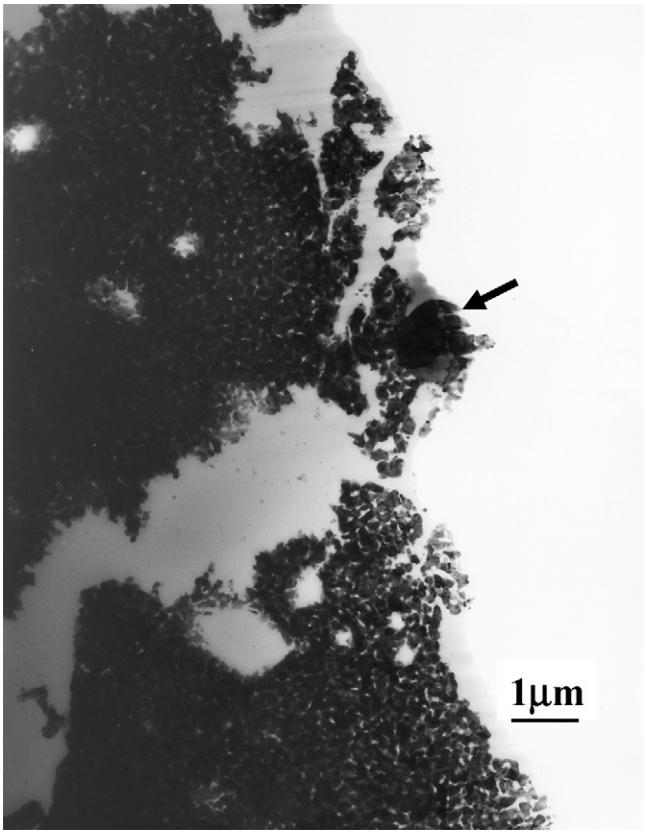


Fig. 9. Bright field TEM image of $CuFe_2O_4$ reduced with $H_2$ at 350 °C. The arrow in the figure indicates a large metallic Cu grain.

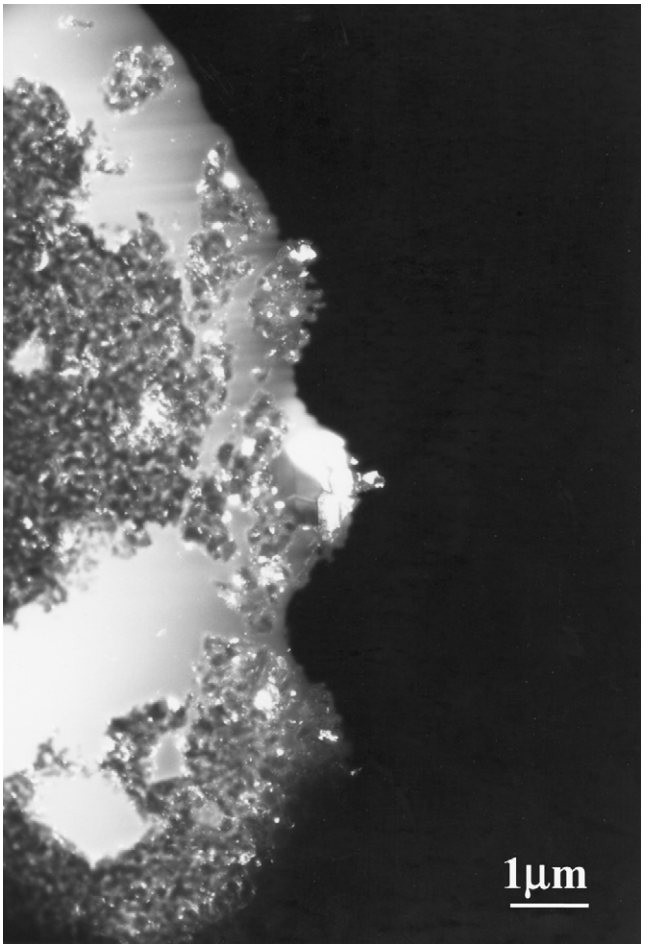


Fig. 10. Dark field image of $CuFe_2O_4$ reduced at 350 °C.

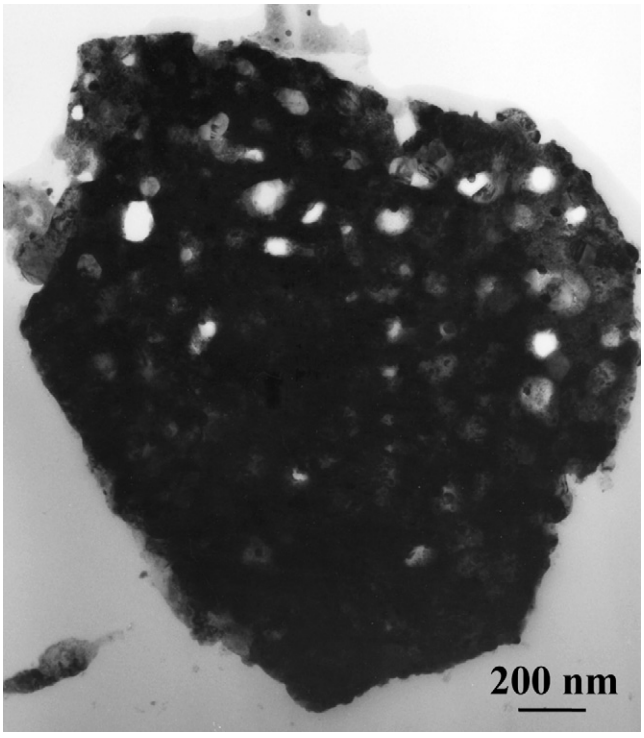


Fig. 11. TEM image of a particle with aggregated grains in $CuFe_2O_4$ reduced at 350 °C.

obtained from the image in Fig. 6 (region b) and was attributed consistently to $CuFe_2O_4$ spinel (JCPDS: 25-0283). The reduced phase of magnetite $Fe_3O_4$ also crystallizes in the spinel structure (inverse spinel type) which could not be distinguished because of the close lattice constant and structure with the host spinel. It is noted in the diffraction pattern of Fig. 7c that the weak super-lattice reflections were observable at every one-third position in-between the fundamental lattice reflections from the original copper–iron spinel. This indicates that the structure of reduced spinel phase was analogous to the original spinel structure, but long range periodicity was introduced with its lattice period of 3 times of the original spinel lattice constant. The long periodicity structure was also evident from the high resolution image. This suggests that, with reduction of the original oxidized spinel, defects are systematically introduced to form the super-lattice structure. The reduced sample only consisted of the above-mentioned three phases, i.e., metallic Cu, original spinel, and spinel phase with the super-lattice structure.

Based on the above-mentioned diffraction information, the lattice image of the sample was further analyzed. The high resolution image from polycrystalline region is shown in Fig. 8 which contained regions with different lattice images. The region near the region a in Fig. 6 was further enlarged to observe the special relation of the atomic array and structure at the interface between deposited Cu and oxide. The deposited Cu particle was located on the spinel phase with super-lattice structure. The atomic arrays in these two regions were represented by the straight lines in the figure. The directions of the arrays for these two phases matched to each other. The lattice spacing of the Cu particle is suggested to be fitted to that of the spinel super-lattice. This means that the interface between Cu and oxide is not merely physical contact, i.e., suggesting strong chemical interaction of reduced oxide and deposited metallic Cu in the vicinity of the interface regions.

### 3.3. Copper–iron spinel oxide reduced at 350 °C

The $CuFe_2O_4$ spinel catalyst more deeply reduced at 350 °C with hydrogen was observed by TEM. The reduction temperature was the same as the reaction temperature for reforming of DME; i.e., the textural and chemical states appear to be close to the operating condition. The bright field and dark field images in low magnification and high resolution were observed. The bright field image of Fig. 9 consisted of a number of agglomerated particles. The size of each particle was *ca.* 100 nm. The large single crystalline oxide particles in Fig. 3 were no longer observed, whereas metallic Cu particles grown to *ca.* 1 μm were often observed (indicated by an arrow). Although many particles were aggregated, most of the particles were separated by cracks. This means that the reduction at high temperature destroyed the original large particle of spinel oxide into pieces.

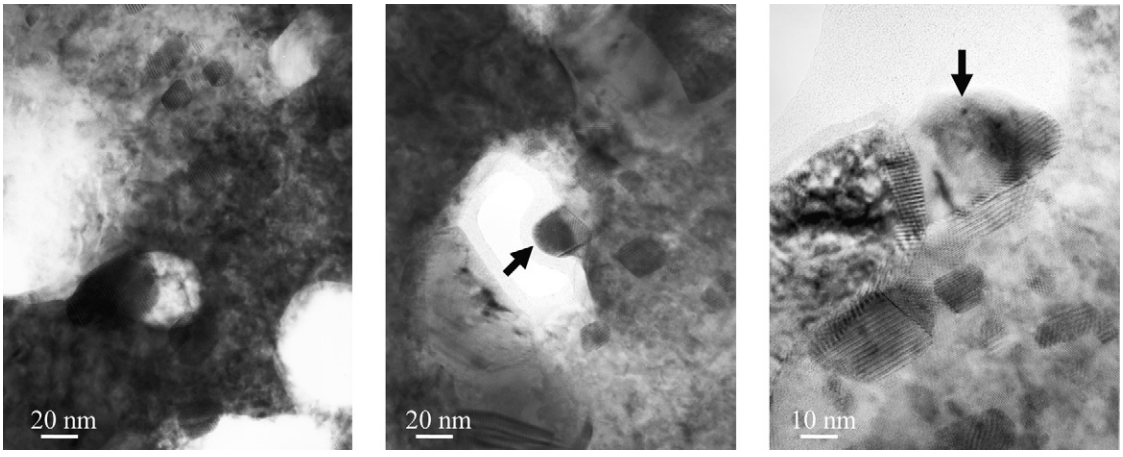


Fig. 12. Typical HR-TEM images of $CuFe_2O_4$ reduced at 350 °C. The arrows in the figure indicate metallic Cu grains.

The dark field image of Fig. 10 obtained from the Cu diffraction indicated that the sample also contained fine deposits of copper. Although exceptionally large Cu particles were contained, most of the Cu deposits were smaller than 100 nm. These fine Cu deposits were dispersed on the remaining dark particles that could be ascribable to reduced oxides. The X-ray diffraction patterns of $CuFe_2O_4$ after reduction at 350 °C consisted of only Cu metal and $Fe_3O_4$, but oxides of copper such as CuO and $Cu_2O$ were not detected [22].

Fig. 11 shows a typical particle with its size of 1 μm which included a number of voids in the particle. The micrograph indicates that the particle consisted of a number of aggregated fine particles to constitute an extremely porous microstructure. A great number of metallic copper particles were observable as those without voids in the particle, since voids were formed only in the oxides upon reduction and elimination of Cu components. As compared with the sample reduced at 250 °C, the sample reduced at 350 °C exhibits a number of metallic Cu particles deposited and grown in size. The voids also gained their size with increasing reduction temperature as shown in Fig. 11. The whole particle is sponge-shaped structure with a number of primary particles and pores.

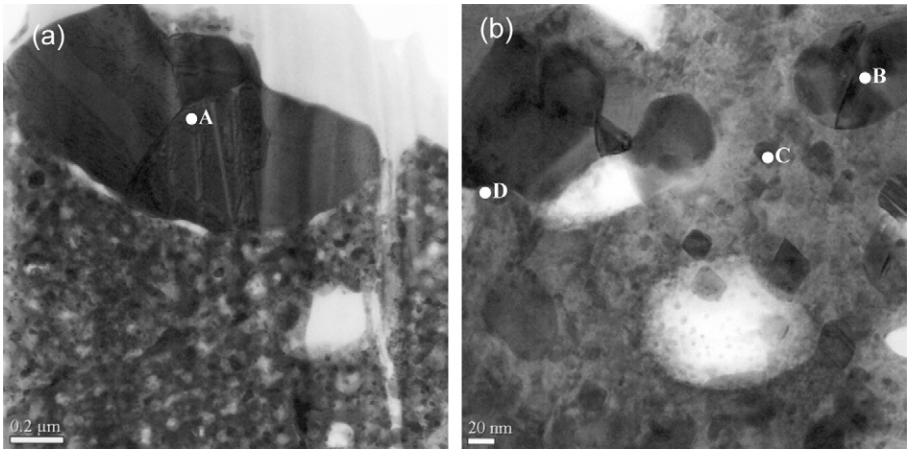


Fig. 13. STEM image of $CuFe_2O_4$ reduced at (a) 250 °C and (b) 350 °C. Spots A-D are analysis points for EDX.

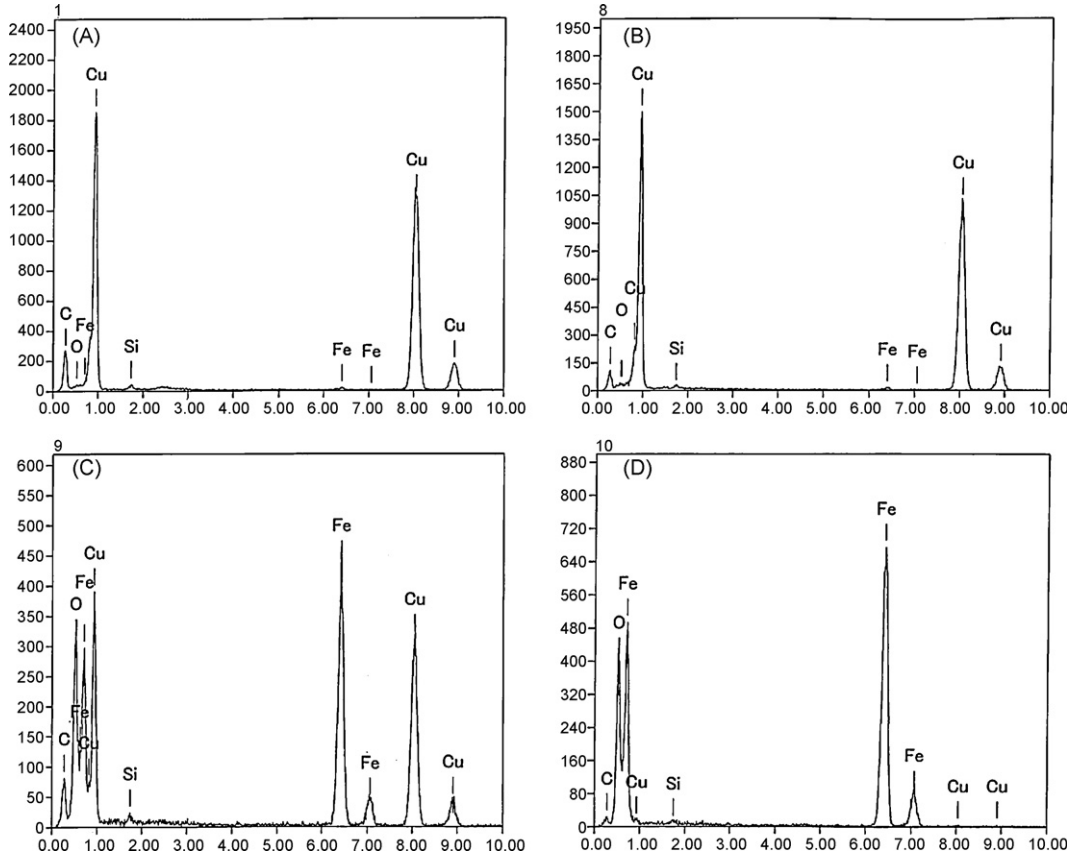


Fig. 14. EDX spectra for the designated positions (A-D) of reduced $CuFe_2O_4$ in Fig. 13.

Fig. 12 shows some typical images obtained by magnification of Fig. 11. The high resolution image was obtained for the regions near the pores. Despite the complicated morphology of the particle, the high resolution image only consisted of crystalline regions of small crystallites with the size ranging 5–30 nm. The pores were found to be 10–100 nm in size. The examples of Cu particles were shown by the arrows in the micrographs. The crystallinity of each particle was high for the sample reduced at 350 °C as in that reduced at 250 °C, though the size of each particle which generally consisted of single grain was decreased. Selected area diffraction patterns obtained from this region could be attributed to Cu. The diffraction patterns of oxides could be ascribed to spinel oxide judging from the diffraction pattern as in the case of the sample reduced at 250 °C. The difference between $Fe_3O_4$ (inverse spinel) and original $CuFe_2O_4$ spinel was unclear. Although the super-lattice structure with 3-fold lattice parameter was frequently observed for the sample after reduction at 250 °C as explained in Section 3.2, this phase was not observed for the sample reduced at 350 °C. The phase with superstructure appears to be formed only in the intermediate stage of the reduction and converted to reduced iron oxide $Fe_3O_4$ after reduction at 350 °C. At the intermediate stage of the reduction process, spinel, metallic copper, and reduced iron oxides appeared to coexist [22].

### 3.4. STEM–EDX analyses

Fig. 13a and b shows the bright field STEM image of the $CuFe_2O_4$ sample reduced at 250 °C and 350 °C, respectively. Large particles of *ca.* 1 μm in size were sometimes observed for both samples, which are attributed to the well grown single crystalline Cu particles. Only metallic copper particles have grown significantly and size of other grains ranged from a few nm to 100 nm. The small grains will be attributed to spinel in oxidized and reduced state, and metallic Cu, on the basis of the discussion in Section 3.2.

The reduced samples were subjected to the composition analysis at points A to D by an energy dispersive X-ray analyzer (EDX, Fig. 14). The EDX spectra for points A and B exhibited the line ascribable to Cu, whereas other metal component and oxygen were not detected. Thus, this grain region is attributed to metallic Cu grown on reduction without crack formation. The other part was composed of the oxygen and metallic components. The point C consisted of Fe and O rich phases without Cu. But another point analysis for D gives the composition of Cu, Fe, and O. These regions may be ascribable to Fe oxide, probably magnetite, and spinel phase with their size of *ca.* 50–100 nm, respectively. In addition to these two regions some voids were coexisted. The single crystalline

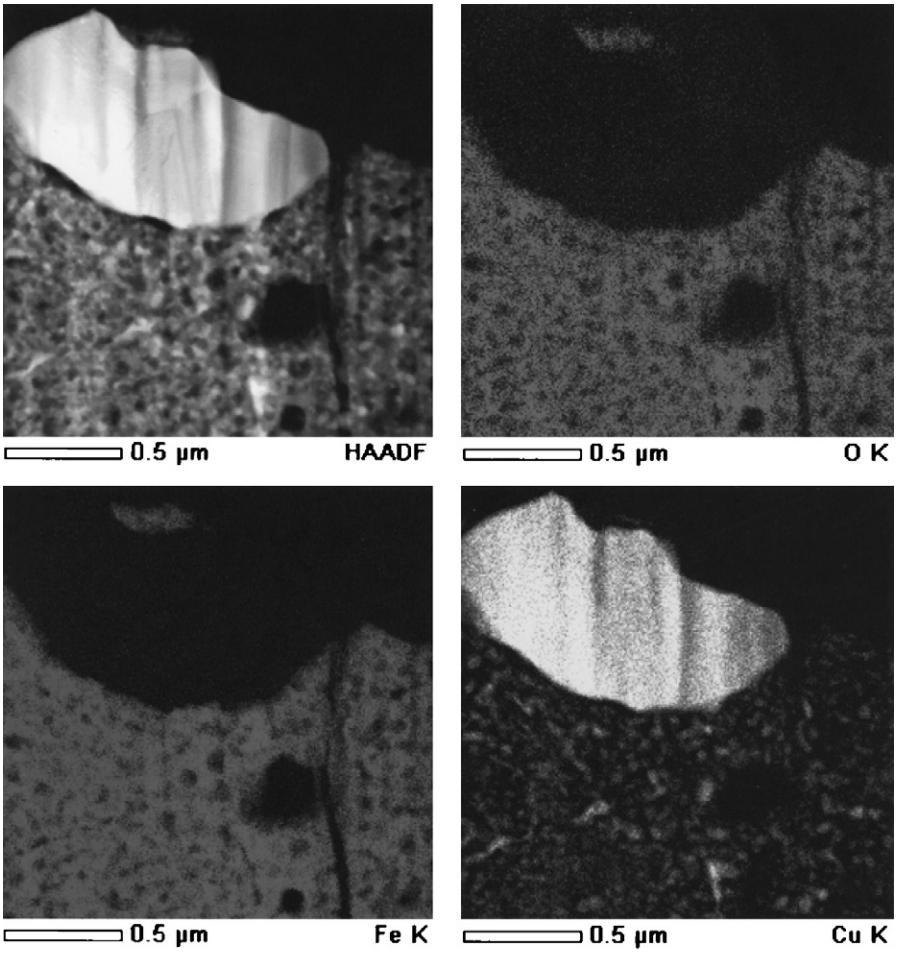


Fig. 15. HAADF and X-ray images of O, Fe, and Cu of $CuFe_2O_4$ reduced at 250 °C.

particle and wide voids of a few nm were observable in the aggregate.

The compositional differences were more clearly distinguished from corresponding high angle annular dark field (HAADF) image of the sample reduced at 250 °C as shown in Fig. 15. The HAADF image contrast is strongly dependent on the average atomic number of the region. Thus, the compositional difference was clearly judged from the image. The X-ray mapping of the corresponding region is also shown in Fig. 15. It is clear from the contrast of the large Cu grain that the bright HAADF contrast corresponds to metallic Cu in which Fe and O were scarce from the X-ray mapping. The Cu-containing small grains were also observable from the X-ray image of Cu. The sample reduced at 250 °C often contained a large extent of overlapping part of Cu and Fe. However, the iron containing part mostly accompanied the oxygen, i.e., the iron is mostly present as the oxide phase. It is clear that the sample consisted of compositional heterogeneity because of the phase

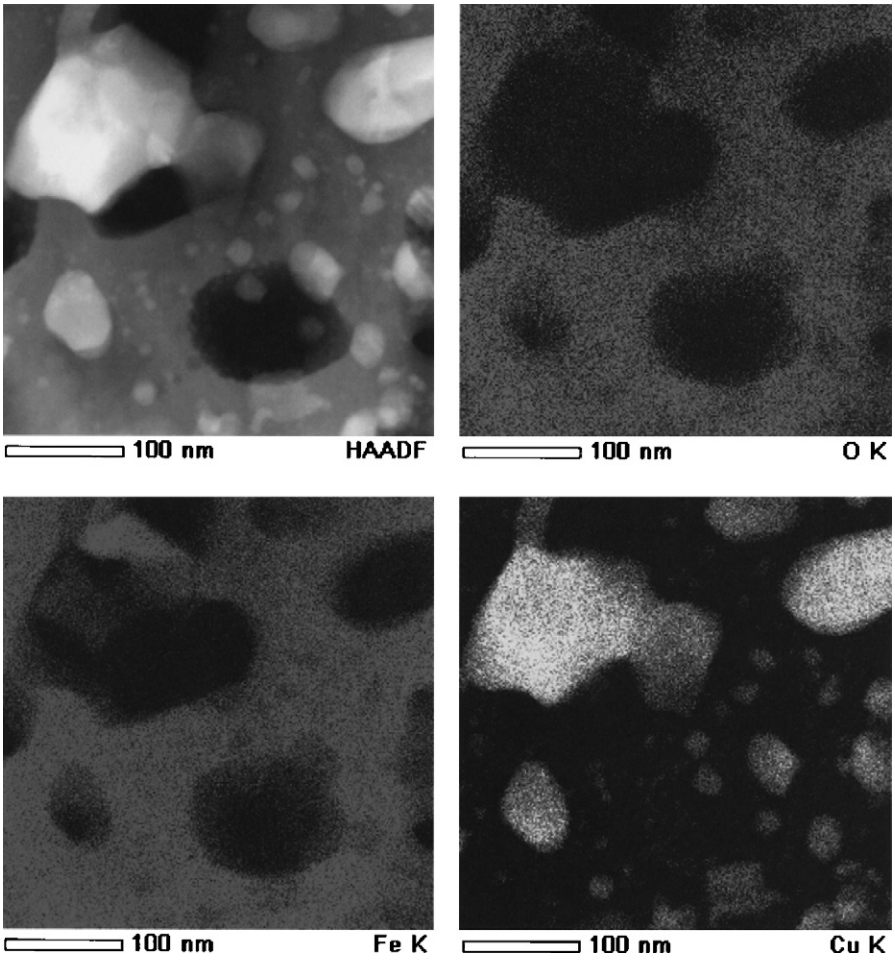


Fig. 16. HAADF and X-ray images of O, Fe, and Cu of $CuFe_2O_4$ reduced at 350 °C.

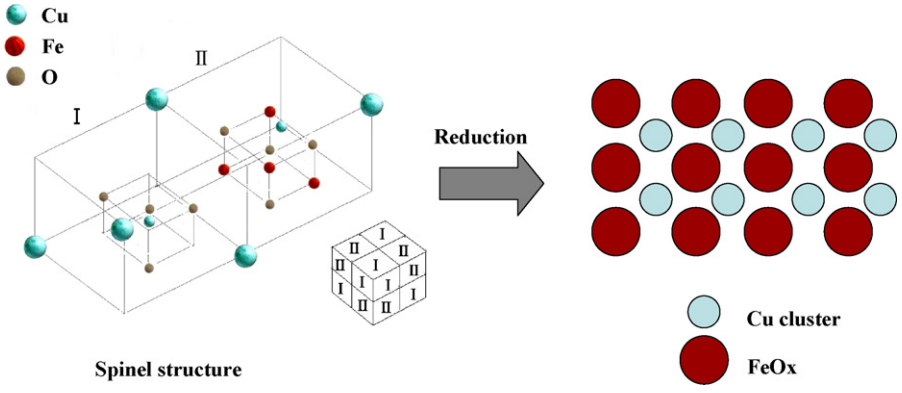


Fig. 17. Schematic diagram for reduction process of $CuFe_2O_4$ spinel and formation of Cu deposits.

separation and reduction. The size of the each grain was not uniform, ranging from 5 to 30 nm. The large fraction of the parts composed only of Fe and O means that, during the phase separation process, Cu is eliminated from iron-rich spinel oxide upon reduction, leading to formation of fine particles on the host oxide. Although large single crystalline Cu was observed, most of the Cu particles were fine and expected to be active for the catalytic reaction.

The sample heated at 350 °C was different in microstructure from that at 250 °C (Fig. 16). Magnified HAADF and EDX mapping images indicated clear separation of Cu metal and Fe oxide phase. The sizes of each grain of Cu and iron oxide are *ca.* 50–100 nm. HAADF–STEM image indicated obviously grown Cu particles like those in Fig. 13, whereas other parts became more porous as compared with the sample reduced at 250 °C. The corresponding compositional image also confirmed porous microstructure and well developed separation of phases. It is indicated that the sample contained the parts with Fe and O, which were well separated from those containing Cu.

### 3.5. Reduction process of $CuFe_2O_4$-based spinel

The reduction process of $CuFe_2O_4$-based spinel was schematically shown in Fig. 17. As previously reported [7,13,17], the sample pre-calcined in air below 900 °C was less active for methanol steam reforming step (1) in DME SR than those heated at 900 °C and 1000 °C. The BET surface area after heating at or higher than 900 °C was very small (*ca.* 1 $m^2\ g^{-1}$). The particles are grown in size during complete solid state reaction between copper oxide and iron oxide to form $CuFe_2O_4$ spinel. During the calcination in air at elevated temperatures, the Cu and Fe atoms are accommodated to respective cationic sites in the spinel structure; i.e., atomic dispersion was achieved at this stage. The oxidation states of copper and iron are di- and tri-valent, respectively. After reduction with hydrogen at 250 °C or 350 °C, however, these oxidation states are no longer stable. Copper is readily reduced to metallic state and iron oxide to $Fe_3O_4$ with inverse spinel structure. Metallic iron was also observed for the sample reduced at 350 °C, though the fraction was small. Formation of these phases accompanies separation of two components and volume shrinkage. The large extent of textural modification and the pore formation were observed by TEM. The comparison of the reduced samples at 250 °C and 350 °C clearly indicated that, upon reduction, the phase separation and pore formation were progressed. This microstructural change agreed with that of surface area upon reduction. Deposited Cu grains should be small in size at the initial stage of the reduction, but grown in size with a further progress of reduction. However, strong chemical interaction of deposited Cu and the host spinel oxide could be expected from this study. Thus, the Cu deposits remain small in size as compared with the Cu catalysts prepared by impregnation on an inert support. The growth of the Cu particles is one of the main causes of the degradation in Cu-based catalysts for DME reforming. The main factors for deactivation of $CuFe_2O_4 + \gamma$-alumina are deposition of carbonaceous species and sintering of Cu. Especially, in the reaction at or higher than 350 °C, thermal degradation with sintering is dominated. Therefore, the preparation of Cu catalyst from the spinel oxide via phase separation should be effective in maintaining the fine metallic state of Cu, though the overall BET surface area is small.

## 4. Conclusions

High resolution transmission electron microscope and scanning TEM with EDX analysis were proven to be powerful tools for observation of formation process of the active phase in the spinel-based oxide. Strong chemical interaction between deposited Cu and the host oxide could be obvious from the intimate contact and lattice matching at the interface. Although impregnation of Cu on alumina support has been well established, such strong chemical interaction cannot be expected for impregnated catalysts. The reduced spinel catalyst composed of number of small grains of Cu and the host spinel oxide and resultant iron oxide was highly porous and crystalline. A large extent of rearrangement of microstructure in addition to the metal deposition is the reason for the high dispersion and catalytic activity. Though the spinel formation was accomplished at very high temperature of 900 °C in the present study, the reduction in hydrogen at *ca.* 350 °C completely decomposed the sintered body to provide a new active surface of Cu for the catalysis. The catalyst microstructure observed in the present study was not optimized, since largely grown metallic copper particles were often observed in addition to the fine copper deposits. Precise control of reduction process and grain size of the deposited Cu further opens the possibility in preparing more active reduced spinel catalyst, since the present catalysts still included largely grown deposits.

## Acknowledgements

The authors would like to thank N. Sugiyama and K. Kurushima (Toray Research Center, Shiga, Japan) for their assistance in TEM observation and analysis.

## References

[1] P.G. Patil, J. Power Sources 37 (1992) 171.
[2] T. Isono, S. Suzuki, M. Kaneko, Y. Akiyama, I. Yonezu, J. Power Sources 86 (2000) 269.
[3] S. Ahmed, M. Krumplet, J. Hydrogen Energy 26 (2001) 291.
[4] A. Bhattacharyya, A. Basu, US Patent 5,498,370 (1996) to Amoco Corporation.
[5] Y. Sato, A. Noda, T. Sakamoto, Y. Goto, SAE Tech paper, 2000-01-1809, 2000.
[6] K. Yamada, K. Asazawa, H. Tanaka, US Patent 6,605,559 (2003) to Daihatsu Motor Co. Ltd.
[7] T.A. Semelsberger, R.L. Borup, Int. J. Hydrogen Energy 30 (2005) 425.
[8] V.V. Galvita, G.L. Semin, V.D. Belyaev, T.M. Yurieva, V.A. Sobyanin, Appl. Catal. A 216 (2001) 85.
[9] K. Takeishi, H. Suzuki, Appl. Catal. A 260 (2004) 111.
[10] T. Matsumoto, T. Nishiguchi, H. Kanai, K. Utani, Y. Matsumoto, S. Imamura, Appl. Catal. A 276 (2004) 267.
[11] T.A. Semelsberger, R.L. Borup, in: Proceedings of the 205th Electrochemical Society Meeting, San Antonio, TX, 2004.

[12] T. Mathew, Y. Yamada, A. Ueda, H. Shioyama, T. Kobayashi, Appl. Catal. A 286 (2005) 11.
[13] Y. Tanaka, R. Kikuchi, T. Takeguchi, K. Eguchi, Appl. Catal. B 57 (2005) 211.
[14] K. Faungnawakij, Y. Tanaka, N. Shimoda, T. Fukunaga, S. Kawashima, R. Kikuchi, K. Eguchi, Appl. Catal. A 304 (2006) 40.
[15] T.A. Semelsberger, K.C. Ott, R.L. Borup, H.L. Greene, Appl. Catal. B 65 (2006) 291.
[16] T.A. Semelsberger, K.C. Ott, R.L. Borup, H.L. Greene, Appl. Catal. A 309 (2006) 210.
[17] K. Faungnawakij, Y. Tanaka, N. Shimoda, T. Fukunaga, R. Kikuchi, K. Eguchi, Appl. Catal. B 74 (2007) 144.
[18] S. Wang, T. Ishihara, Y. Takita, Appl. Catal. A 228 (2002) 167.
[19] M. Nilsson, P. Jozsa, L.J. Pettersson, Appl. Catal. B 76 (2007) 42.
[20] Y. Tanaka, T. Takeguchi, R. Kikuchi, K. Eguchi, Appl. Catal. A 279 (2005) 59.
[21] Y. Tanaka, T. Utaka, R. Kikuchi, T. Takeguchi, K. Sasaki, K. Eguchi, J. Catal. 215 (2003) 271.
[22] K. Faungnawakij, R. Kikuchi, T. Matsui, T. Fukunaga, K. Eguchi, Appl. Catal. A 333 (2007) 114.